Flinders
UNIVERSITY

Dynamical (e,2e) Studies of Bio-Molecules

Joseph Douglas Builth-Williams

Submitted in fulfillment for the requirements
of the degree of Masters of Science

March 2013

School of Chemical and Physical Sciences
Flinders University of South Australia

The most exciting phrase to hear in science, the one that heralds the most discoveries, is not "Eureka!" (I found it!) but "That's funny..."

∼ Isaac Asimov (1920-1992)

4

Measurements on Pyrimidine

4.1 Introduction

Pyrimidine, otherwise known as 1,3-Diazine, is a hetrocyclic aromatic organic compound that bears a structural resemblance to benzene and pyrazine. Pyrimidine, as its alternative name suggests, is a member of the diazine family of molecules and it incorporates two nitrogen atoms located at positions 1 and 3 on its ring (see Figure 4.1). The boiling point of pyrimidine is 396K and its melting point is around 293K - 295K, implying that at room temperature it forms a clear fluid. The chemical formula of pyrimidine is $C_4H_4N_2$, it has a molar mass of $80.088 gmol^{-1}$ and a density of $1.016 gcm^{-3}$.

4.1.1 Significance of this Molecule

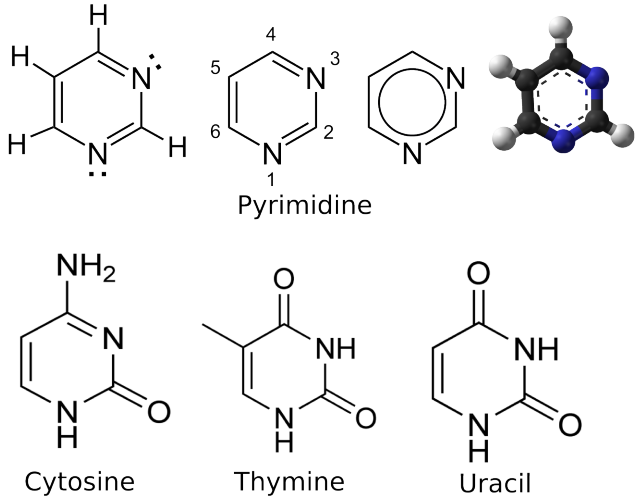

Figure 4.1: *Pyrimidine and its relevant nucleobase derivatives: Cytosine, thymine and uracil. Various representations of pyrimidine can be seen in the top row.*

As mentioned in Section 1.2, DNA forms the basis for all life, acting as a blueprint that encodes for the various proteins. DNA's ability to act as a medium for genetic information is achieved through the existence of four chemicals, known as the nucleobases: adenine, guanine, cytosine and thymine. As expected, the bases are structurally similar and can be derived from two precursor molecules: purine for adenine and guanine; and pyrimidine for cytosine and thymine, as well as the RNA specific base uracil (which replaces thymine). This can also be seen in Figure 4.1. Thus pyrimidine, as the precursor molecule to half of the known nucleobases, is an important molecule to study if the biological effects of radiation are to be fully understood.

Experimentally, there have been a number of previous studies undertaken on pyrimidine, using techniques such as photoabsorption spectroscopy [98, 99, 100, 101, 102] and photoelectron spectroscopy [103, 104, 105, 106, 107], but the most significant, in respect to this thesis, was the EMS study conducted by Ning *et al.* [108]. Ning *et al.* performed EMS measurements, using what is commonly known as the Weigold configuration [2] (i.e. a non-coplanar symmetric geometry, see Section 2.4) and 600 eV incident electrons. The outcome of that study was a measurement of the momentum distributions of the outer valence orbitals of pyrimidine and a binding energy spectrum [108]. Furthermore the data collected by Ning *et al.* was finally able to put the controversy, as to whether the $7b_2$ or the $2b_1$ orbital was the Highest Occupied Molecular Orbital (HOMO), to rest, finding that the $7b_2$ orbital was the HOMO [108].

4.2 Binding Energy Spectrum

A Binding Energy Spectrum (BES) was initially measured in order to provide an overview of the necessary scattered electron energies required to perform TDCS measurements on any particular molecular orbital. In addition, the BES also enabled us to probe information pertaining to the valence electronic structure of this molecule. The BES for pyrimidine is shown in Figure 4.2, and is, in fact, an aggregate of the numerous binding energy spectra taken throughout the experiment. During each BES measurement, the ejected and scattered analysers was held at 70° and 15° respectively, while the incident and ejected electron energies were held at 250eV and 20eV respectively. The scattered electron energy was scanned across a range of energies in 0.3eV steps, from which the binding energy was calculated using energy conservation.

The BES was fitted with nine Gaussians (see Figure 4.2), each of which is labelled with the appropriate orbital shells that they represent. Those assignments

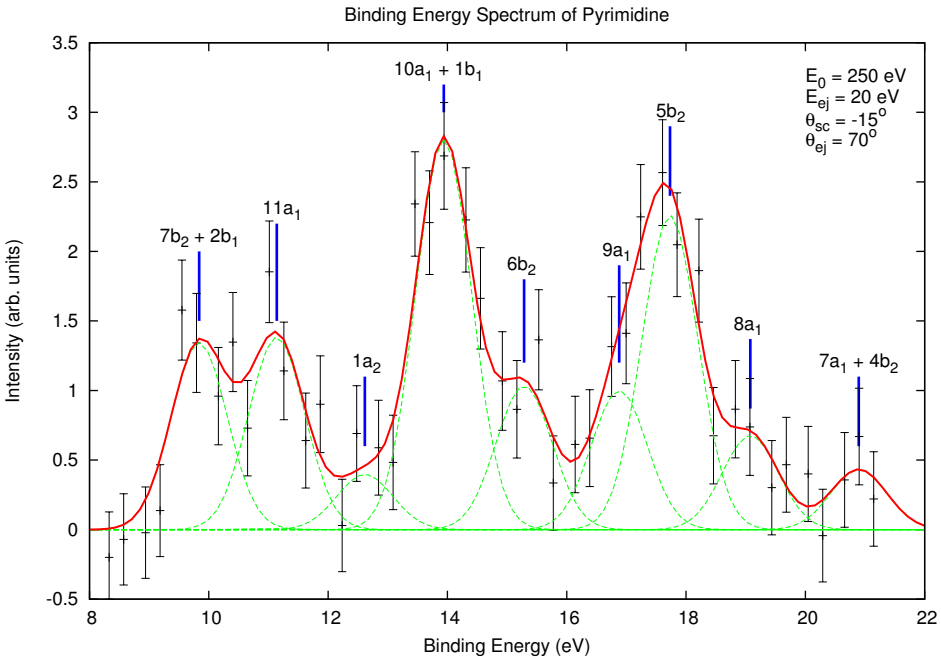

Figure 4.2: *The complete Binding Energy Spectrum of Pyrimidine in the range of* $8 - 22eV$*. The green dashed lines represent the individual Gaussians, while the solid red lines is the sum of the Gaussians.*

were based upon the BES data published by Ning *et al.* [108], that was composed of results determined using electron momentum spectroscopy (EMS) and photoelectron spectroscopy (PES), and calculated using a number of different theoretical models including Hartree-Fock (HF), density functional theory with a standard hybrid Becke, three-parameter, Lee-Yang-Parr (B3LYP) exchange-correlation functional and the Outer Valence Green's Function (OVGF) approach. All these results and the orbital assignments are summarised in Table 4.1.

It should be noted here that it is usual for the Gaussian widths in (e,2e) spectroscopic experiments to be a convolution of the instrumental energy resolution and the natural orbital shell widths, Γ, which are obtained from the PES data. However in the case of pyrimidine it was found that the binding energy resolution of $\Delta E_{BE} = 1.1$eV, Full Width Half Maximum (FWHM), a little better than that obtained with the example helium spectrum shown in Figure 3.13, was sufficient for the fitting software [109] to produce a good overall representation of the BES (see the solid line in Figure 4.2). This approximation was applicable here as $\Delta E_{BE} >> \Gamma$ is true for each orbital. A complete summary of the results from the fitting algorithm can be seen in Table A.1 in Appendix A.

Like a number of other biomolecules [15, 35, 36, 38], pyrimidine has a complex

Table 4.1: *Ionisation potentials of pyrimidine in eV, taken from the work of Ning et al. [108]. The (e,2e) column is data from the current work.*

Orbital	PES	EMS	(e,2e)	HF	B3LYP	SAOP	OVGF	ADC(3)
$7b_2$	9.8	9.8	9.8	11.34	7.29	10.29	9.83	9.49 (12a')
$2b_1$	10.5	10.5		10.32	8.19	11.50	10.40	10.37 (3a")
$11a_1$	11.2	11.3	11.1	12.92	8.60	11.53	11.36	10.93 (11a')
$1a_2$	11.5		12.6	11.56	9.04	12.30	11.28	11.20 (2a")
$10a_1$	13.9	14.1	13.9	16.00	11.55	14.27	14.49	14.40 (1a")
$1b_1$				15.77	11.76	14.91	14.49	14.42 (10a')
$6b_2$	14.4		15.3	16.25	12.00	14.49	14.63	14.63 (9a')
$9a_1$	15.8	15.7	16.9	17.76	13.09	15.79	16.25	16.26 (8a')
$5b_2$	17.0	17.5	17.7	19.18	14.39	16.92	17.26	17.55 (7a')
$8a_1$	17.7		19.1	20.16	15.00	17.56	18.25	18.11 (6a')
$7a_1$		20.6	20.9	24.31	18.24	20.60		
$4b_2$				24.41	18.27	20.65		
$6a_1$		24.5		29.32	21.95	24.13		
$3b_2$		26.2		32.62	24.61	26.62		
$5a_1$		29.3		35.82	27.25	29.11		

orbital structure comprising 15 molecular orbitals, only 12 of which are visible in Figure 4.2 (see Table 4.1 for a complete listing of the orbitals). As there were only nine Gaussians fitted to the BES, it is clear that three of the twelve molecular orbitals aren't resolved enough to form their own distinct peaks. As a consequence, they instead contribute to other peaks and so have been merged with their closest neighbour ($2b_1$ with $7b_2$, $1b_1$ with $10a_1$ and $4b_2$ with $7a_1$). Eight of the nine resolved peaks in Figure 4.2 are representative of the outer valence region of the molecule (i.e. $E_{BE} \lessapprox 20$eV), while only a single resolved peak lies in the inner valence region of the molecule (i.e. $E_{BE} \geq 20$eV) for the binding energy range we accessed in this study.

It should be noted that the Highest Occupied Molecular Orbital (HOMO) of pyrimidine is the $7b_2$ orbital. However this is not without some contention, as the Hartree-Fock (HF) approximation actually assigns the HOMO to the $2b_1$ orbital but Ning *et al.* found significant evidence to the contrary [108]. This highlights the limitations in the HF approach in calculating orbital energies and assignments. Another peak of note is the $10a_1$ orbital that is located at 13.9eV, which represents the maximum intensity in the BES. The $10a_1$ orbital intensity is likely to contain contributions from the $1b_1$ orbital, which, in itself, is difficult to resolve as a separate peak due to both those orbitals having very similar binding energies (see Table 4.1). Spatial orbital representations of the $7b_2$ and the $10a_1$ orbitals can be seen in Figure 4.3.

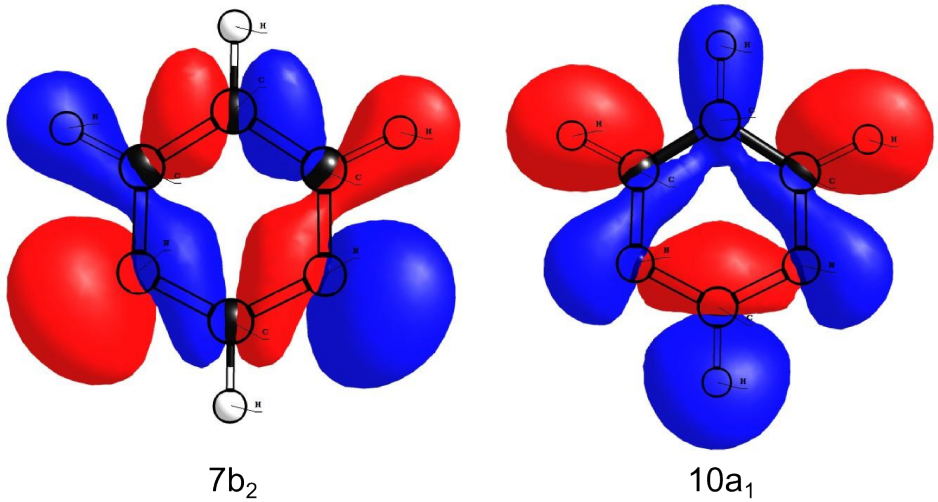

Figure 4.3: *A spatial orbital representation of both the* $7b_2$ *orbital and the* $10a_1$ *orbital of pyrimidine. These models were produced using Avogadro [110] and GAMESS [111].*

4.3 Experimental Considerations

The sample used in the present study was of stated purity greater than 99% and was purchased from Sigma-Aldrich, Australia. However, as the sample was transferred into the glass sample vessel (see Figure 3.1), it was exposed to air and thus a number of gaseous contaminants. In order to eliminate these contaminants within the sample, it underwent three freeze-pump-thaw cycles. The pyrimidine is first frozen by immersing the glass sample vessel in liquid nitrogen, after which it is exposed to a vacuum. At first this vacuum is achieved by using a secondary rotary vacuum pump, but after a while that pump is switched off and the vacuum in the scattering chamber is used to further evacuate the glass vessel. This is done as the turbomolecular pump on the vacuum chamber produces a significantly better vacuum compared to the rotary vacuum pump ($\sim 1 \times 10^{-8}$torr compared to $\sim 1 \times 10^{-2}$torr). Finally the sample is thawed with minimum interaction, allowing the gaseous contaminants to degas from the sample (and eventually be removed in the next pump cycle).

According to Nuevo *et al.*, pyrimidine has a tendency to photolytically decompose into uracil when exposed to UV light and water [112]. Precautions were therefore taken during the experiment to minimise the samples exposure to UV light, by covering the sample vessel with aluminium foil. In general, pyrimidine is volatile enough to ensure a sufficient density in our molecular beam, for the (e,2e) experiments. However, as noted by Ning *et al.* [108], the valve and needle did require some heating in order to ensure that pyrimidine did not condense, and thus cause any noticeable pressure fluctuations during the course of the

measurements.

4.4 Results and Discussion

Presented in this section are four TDCSs for pyrimidine; one for the $7b_2$ (HOMO) orbital and three for the $10a_1$ orbital. Each TDCS was measured at an intermediate incident electron energy of 250 eV, and an ejected electron detection energy of 20 eV. The scattered analyser was held at $-15°$ for the $7b_2$ orbital and for the $10a_1$ orbital it was held at $-5°$, $-10°$ and $-15°$. The ejected analyser was moved through a range of angles in $5°$ steps, over the $55° - 120°$ range, limited by the physical constraints imposed by the (e,2e) spectrometer components (see Section 3.1.4 and Figure 3.6 in particular).

It should be noted that for the TDCS measurements on the $10a_1$ and the $7b_2$ molecular orbitals of pyrimidine there are contributions from the $1b_1$ and $2b_1$ orbitals respectively. These contributions from the $1b_1$ and $2b_1$ orbitals have likely contaminated the observed experimental results and may be a factor in any observed dissonance between the experimental and theoretical results presented in this chapter. From the PES measurements from Potts *et al.* [106], and the EMS measurements of Ning *et al.* [108], it can be seen that the $2b_1$ orbital is of a smaller magnitude than the $7b_2$ orbital of pyrimidine and is offset to a slightly higher binding energy. This would suggest that the contributions from the $2b_1$ orbital will be small in size. However, for the $1b_1$ orbital, both Potts *et al.* and Ning *et al.* have difficulty distinguishing it from the $10a_1$ orbital. Without any experimental results, it is hard to say the amount of contribution this orbital has to the $10a_1$ orbital, though the measurements are thought to be predominantly due to the $10a_1$ orbital [37]. For the sake of simplicity, the TDCS measurements will be referred to by what is thought to be the dominant orbital (i.e. $7b_2$ and $10a_1$) from this point onwards, though it should be remembered that there are contributions from the unresolved orbitals.

Table 4.2: *The current binary to recoil peak (B-R) ratios found in the present study for the $10a_1$ and $7b_2$ orbitals of pyrimidine.*

Orbital	Angle	B-R ratio	Error
$7b_2$	15°	3.776	±1.105
$10a_1$	5°	2.005	±0.348
	10°	4.738	±1.707
	15°	6.670	±3.152

Figures 4.4 and 4.5 thus present the experimental results measured in the cur-

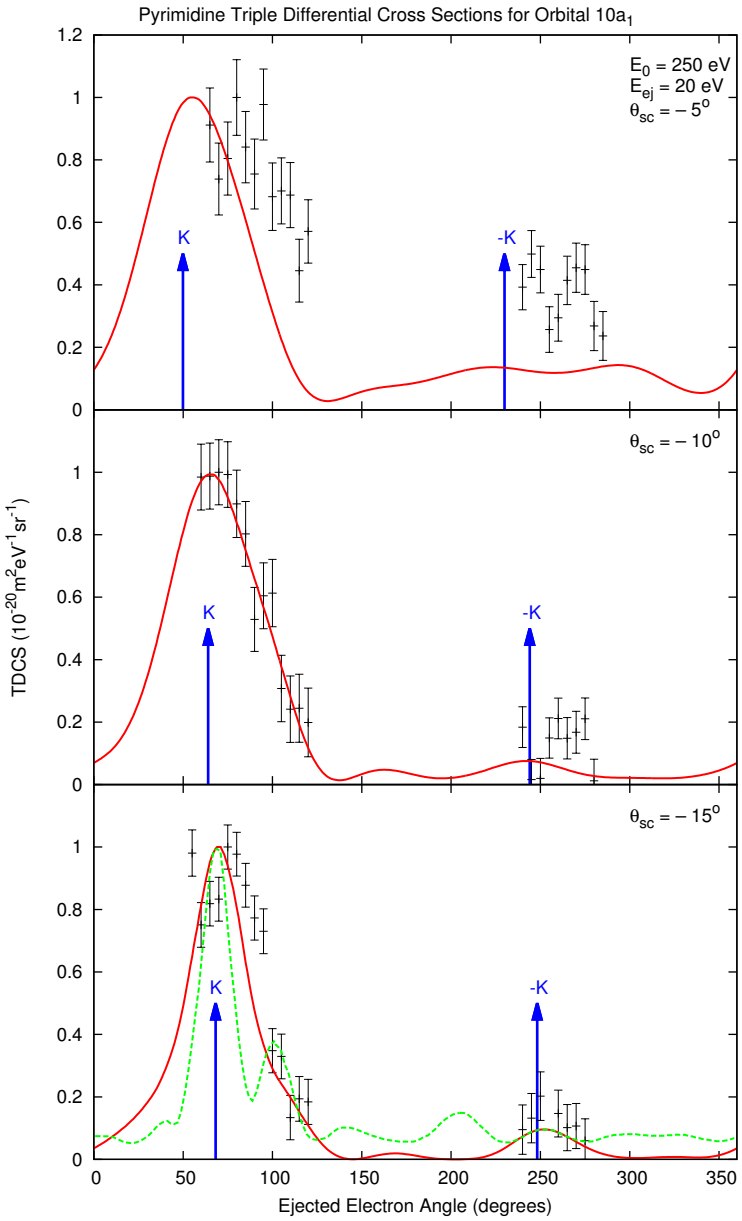

Figure 4.4: *TDCS of the* $10a_1$ *orbital of pyrimidine, measured at scattered electron angles of* $-5°$, $-10°$ *and* $-15°$, *where* $E_0 = 250$ *eV and* $E_{ej} = 20$ *eV. Also shown are the M3DW results when the molecular wave function is averaged (solid red line) and M3DW results when the absolute value of the molecular wavefunction is averaged (green dashed line). Note, the angular uncertainties on the experimental measurements is* $\pm 2.5°$.

rent study. As the collected TDCS data are relative, they have been normalised to a value of 1 at $\theta_b = 75°$ for the $10a_1$ orbital and the scattered electron angles of $-15°$ and $-10°$, and at $\theta_b = 80°$ for the scattered electron angle of $-5°$. For the $7b_2$ orbital a value of 1 was assumed for $\theta_b = 80°$. Tables of this experimental data, after normalisation, can be found in Appendix A (specifically

Tables A.2, A.3, A.4 and A.5). Note that the actual value of θ_b used in the normalisation is not crucial to the discussion that follows.

As can be seen in the first panel of Figure 4.4 ($\theta_{sc} = -5°$), the measured TDCS has a rather wide binary peak, and its recoil peak has a relatively large magnitude (compared to the other panels). It should also be noted that both the binary and recoil peaks are offset from the momentum transfer direction $\theta_{\vec{\kappa}}$ (represented in the TDCS as $\vec{\kappa}$ and $-\vec{\kappa}$, see Section 2.4 for more information), possibly suggesting the involvement of post-collision-interaction (PCI) effects in the scattering dynamics at $\theta_{sc} = -5°$. Additionally, we further note that because of interference from the primary electron beam experiments at such a small scattered electron angle can be difficult to perform, which is reflected in the TDCS by the scatter in the measured data at all θ_b and by the size of the error bars on each of the TDCSs.

In the second ($\theta_{sc} = -10°$) and third ($\theta_{sc} = -15°$) panels of Figure 4.4 the binary peaks are observed to be relatively narrow, especially that of the $-15°$ case. Similarly, when compared to the $-5°$ case, the magnitude of the recoil peaks displayed by $\theta_{sc} = -10°$ and $-15°$ progressively decreases as does the offset displayed by the measured recoil peak from $\theta_{-\vec{\kappa}}$. However, unlike the $-5°$ measurement, the $-10°$ and $-15°$ TDCS data both display significantly less scatter, especially that of the binary peak $\theta_{sc} = -10°$. Additionally, the error bars displayed on the TDCS in the $-15°$ case are smaller than those measurements taken at the scattered electron angles $-5°$ and $-10°$.

As mentioned above, a curious trend emerges when considering the different panels of Figure 4.4: namely that the magnitude of the recoil peak seems to change as an inverse function of the scattered electron angle. The relative recoil magnitude is usually indicative of the strength of the electron interaction with the molecular nucleus. However the observed behaviour differs to that exhibited by water (H_2O), when studied under the similar kinematic conditions [30]. One interpretation of this observation, put forward by Colyer *et al.* [36], and based upon the works of Al-Hagan *et al.* [113], suggests that this is caused by the location of pyrimidines' centre-of-mass. That theory states that due to the lack of a nuclear charge at the centre-of-mass, larger scattered electron angles will lead to a decrease in the amount of recoil scattering [36]. This theory has also been used to describe similar phenomena that has been observed in the TDCS of formic acid [35], tetrahydrofuran [15, 36] and thymine [15]. More recently, however, an alternative interpretation has been advanced to explain these observations. Xu *et al.* have suggested that the Electron Momentum Density

(EMD) of the studied biomolecules, with the chosen kinematics being close to the Bethe ridge, is the cause for the observed phenomena [114], rather than the differing locations of the centre-of-mass and nuclear charge. Basically, in their view, it is the symmetry of the particular orbital being probed that leads to the asymmetrical observations [114].

Figure 4.4 also compares the $10a_1$ orbital TDCS experimental results, for $\theta_{sc} = -5°$, $-10°$ and $-15°$, with a calculation developed using the Molecular 3-body Distorted Wave (M3DW) approximation under the same kinematics. These calculations were performed by Madison *et al.* [115]; further information about the model can be found in his previous work [36, 75] as well as a precis of it in Section 2.5.3 of this thesis. As can be seen in Figure 4.4, the preferred model is quite successful in predicting the narrow binary peak of the experimental data and the smaller recoil peaks for $\theta_{sc} = -10°,\ -15°$. However, the model is less successful when it comes to $\theta_{sc} = -5°$ as while it does predict a wider binary peak, it doesn't show the same level of quantitative accord that it displays at the larger scattered electron angles. Furthermore the binary peak remains narrower than the measured data, though this observation could be due to the theoretical results being shifted to smaller angles. As mentioned earlier, an inexact PCI model in the M3DW might be the cause of this discrepancy between the experimental measurements and theoretical calculations at $\theta_{sc} = -5°$. In addition it might also be due in part to contributions from the $1b_1$ orbital being relatively more important at $\theta_{sc} = -5°$ compared to $\theta_{sc} = -10°$ and $-15°$.

As described in Section 2.5.3, there exist two methods by which the M3DW calculations are performed: one involves averaging the molecular wave function while the other involves averaging the absolute value of the molecular wave function [75]. The model presented in Figure 4.4, as a solid red line, uses the former approach, while the green dashed line for the $\theta_{sc} = -15°$ case uses the latter approach. From the comparison between the two theoretical methods utilised and the measurements in Figure 4.4, there is some suggestion that the model that averages the molecular wave function is superior, as it provides a better fit to the experimental measurements. Additionally, it should be noted that the M3DW model has some general difficulty in dealing with orbitals that exhibit "p-type" symmetry, of which the $7b_2$ orbital is an example [108]. This means that in Figure 4.5, a two-lobed binary peak should be present in the TDCS. However while the M3DW calculation does show such a "double" peak, its secondary peak is much smaller and offset compared to what the experimental data exhibits, allowing for the uncertainties on the experimental TDCS. Note that even though the M3DW result in Figure 4.5 employed the inferior averaging of

the absolute molecular wave function value approach, this discrepancy would persist if the preferred model results were available. This follows as averaging the molecular wave function for a $7b_2$ orbital of "p-type" symmetry would lead to a zero TDCS [108]. We note that this observation represents a severe limitation with the present M3DW approach.

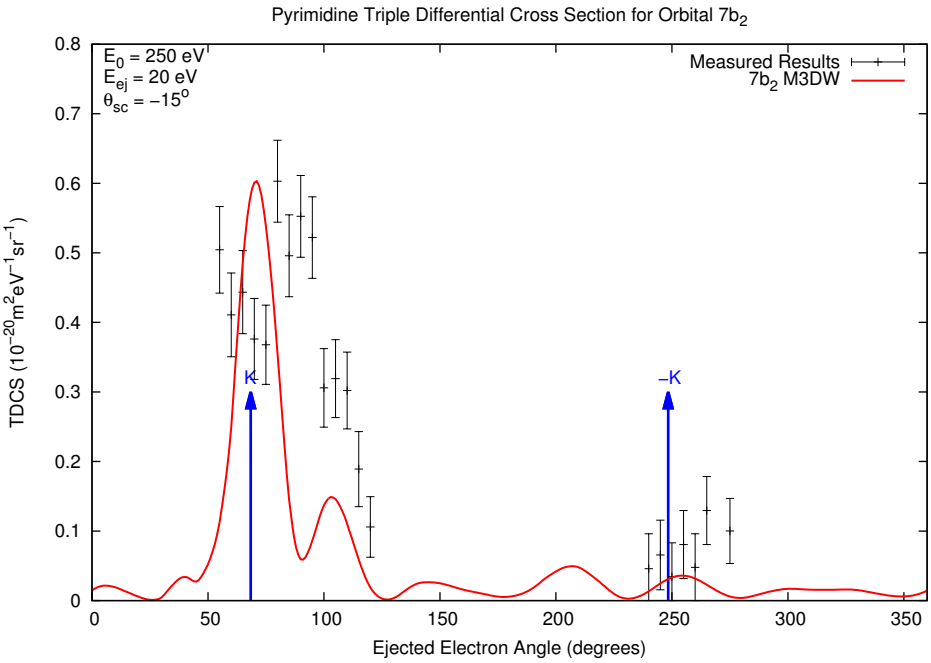

Figure 4.5: *TDCS of the $7b_2$ orbital of Pyrimidine. Note, the M3DW theory represented by the line in this figure involved averaging the absolute value of the molecular wave function.*

The TDCS of the $7b_2$ orbital of pyrimidine, shown in Figure 4.5, has a number of interesting features worth mentioning. The first and foremost would be that the experimental data seems to suggest a double lobed structure in the binary peak, which is what is to be expected from a "p-type" orbital symmetry. However, the significant scatter in the smaller angles of the binary peak makes this observation teneous at best. Furthermore, the $7b_2$ orbital, measured at $\theta_{sc} = -15°$ has a small recoil peak, which is consistant with the previous observations on the $10a_1$ orbital, discussed above.

Finally we note that the measured $7b_2$ TDCS, Figure 4.5, took longer to acquire than those for the $10a_1$ orbital. The reason for this can be seen in Figure 4.2, the (e,2e) intensity of the $7b_2$ orbital is only half that of the $10a_1$ orbital. This means that if all else were equal, save the binding energies, it would take four times longer to achieve the same statistical quality for the $7b_2$ TDCS as

that for the $10a_1$ TDCS. Unfortunately, these experiments are already quite time consuming so that such an option is simply not tenable.

4.5 Conclusion

In this chapter experimental and theoretical dynamical (e,2e) results were presented for the pyrimidine molecule: a molecule of significant biological relevance. As pyrimidine is the precursor molecule for the DNA nucleobases thymine and cytosine, as well as the RNA nucleobase uracil, it acts as a prototype molecule through which the effects of electron interactions with biological matter can be investigated.

While previous studies have probed the valence electronic structure of pyrimidine using other (e,2e) techniques [108], photoabsorption spectroscopy [98, 99, 100, 101, 102] and photoelectron spectroscopy [103, 104, 105, 106, 107], the present investigation represents the first dynamical (e,2e) measurements performed on pyrimidine. Furthermore, the measured binding energies and orbital assignments were found to be in good agreement with the previous studies.

The current TDCS measurements were performed with 250eV incident electrons and 20eV ejected electrons at the scattered electron angles $-5°$, $-10°$ and $-15°$ for the $10a_1$ orbital and at $\theta_{sc} = -5°$ for the $7b_2$ (HOMO) orbital. A narrow binary peak was observed in all the measurements, except that of the $10a_1$ orbital at $\theta_{sc} = -5°$; the most likely reason for this is due to a contribution from the adjacent $1b_1$ orbital, or alternatively it might be indicative of PCI effects influencing the scattering dynamics here.

In addition, it was observed that the recoil peak magnitude, relative to the binary peak, decreased as the scattered electron angle increased: a phenomenum that was not observed to occur in other molecules such as H_2O [30]. Two explanations for why this might be so were discussed in Section 4.4: namely that the observed effect is due to the absence of a nuclear charge at the molecular centre-of-mass [36], or that it is due to the symmetry of the probed molecular orbital [114].

Finally, we found that overall the M3DW calculations are in quite fair agreement with the observed experimental results, particulary when one allows for the complicated nature of the molecular target. This suggests that there is some merit in using the results from M3DW calculations as input for charged-particle track structure simulations [62].